Defense Technical Information Center
Compilation Part Notice

ADP011013

TITLE: Optical Properties of Nanoparticle Pair Structures

DISTRIBUTION: Approved for public release, distribution unlimited

This paper is part of the following report:

TITLE: Materials Research Society Symposium Proceedings Volume 635. Anisotropic Nanoparticles - Synthesis, Characterization and Applications

To order the complete compilation report, use: ADA395000

The component part is provided here to allow users access to individually authored sections of proceedings, annals, symposia, etc. However, the component should be considered within the context of the overall compilation report and not as a stand-alone technical report.

The following component part numbers comprise the compilation report:
ADP011010 thru ADP011040

Optical Properties of Nanoparticle Pair Structures

Marie L. Sandrock, Mahnaz El-Kouedi, Maryann Gluodenis and Colby A. Foss, Jr.[1]
Department of Chemistry, Georgetown University, Washington, District of Columbia 20057.
[1]Current address: Trex Enterprises Corporation, 3038 Aukele Street, Lihue, Hawaii, 96766.
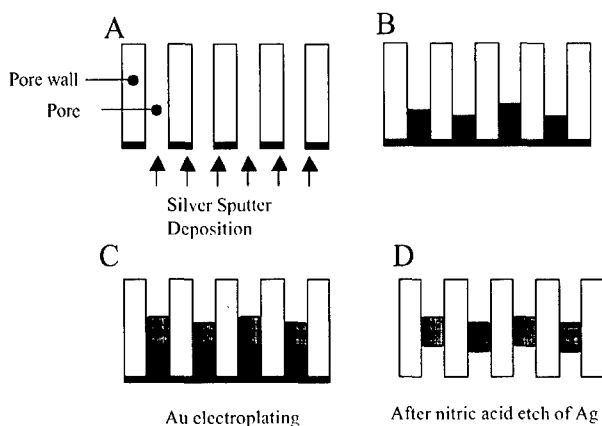
ABSTRACT

The synthesis of nanoparticle pair structures via porous host electrochemical template synthesis reviewed. Electrochemical template synthesis offers two advantages over solution methods, namely: 1) control over particle pair structure and orientation; and 2) control over geometry, size and composition of each member of the particle pair. These features of electrochemical template synthesis allow for straightforward comparison of experimental and theoretical spectra. Orientation control allows for the evaluation of second order nonlinear optical properties of centrosymmetric and non-centrosymmetric nanoparticle pair systems. The dependence of Second Harmonic Generation intensity on particle pair shape size and orientation is discussed. The synthesis and linear spectra of metal-semiconductor nanoparticle pair structures are also discussed, with emphasis on interparticle physical and electromagnetic interactions.

INTRODUCTION

There are numerous methods for synthesizing nanoscopic metal particles, such as bulk solution reduction of metal salts [1,2], electric discharge [3], vacuum deposition [4], and template synthesis [5,6]. Template synthesis involves the use of a host material whose pores define the geometry of the structures grown within it, for example via electrochemical deposition of metals. In the last decade, there has been an increasing interest in the optical properties of nanoscopic metal particle structures, with a keen emphasis on how optical properties depend on particle size, shape, composition, and orientation in the incident field. Electrochemical template synthesis is well-suited for fundamental optical studies on nanoparticle structures because it allows for the control of particle size, shape and orientation. A common porous host material is anodic aluminum oxide, which possesses not only well-defined parallel arrays of cylindrical pores, but is also transparent through most of the visible and near-infrared spectrum.

A number of previous studies have focused on the optical properties of metal spheres and rods grown in porous aluminum oxide [5-9]. In our laboratories, we have extended the electrochemical template synthesis method to metal nanoparticle pair structures, where both members of the pair are spheres or rods of equivalent dimensions, or where the pair structure is non-centrosymmetric (e.g., composed of a sphere and a rod, or two rods of different dimensions). We have been able to examine the linear spectra as a function of particle shape and interparticle spacing [10], and compare the second harmonic generation (SHG) signals produced by centrosymmetric and non-centrosymmetric structures [11]. We have also extended the template synthesis method to pair structures where one member is a metal and the other is a semiconductor [12,13].

In this paper, we review the synthesis of nanoparticle pair structures, and present some of our recent results on the SHG of gold nanoparticle pairs, and the linear spectra of gold/silver iodide nanoparticle pair structures.

A

Pore wall —
Pore —

Silver Sputter
Deposition

B

C

Au electroplating

D

After nitric acid etch of Ag

Figure 1. *Schematic of the electrochemical template synthesis for single particle structures. A. Porous template host is coated with silver to provide a conductive layer. B. With the silver coat as the working electrode, additional silver is deposited electrochemically to form a foundation of silver rods. C. Gold is deposited onto the silver foundation to form gold nanorods. The aspect ratio is controlled by the pore diameter and the amount of gold deposited. D. The silver foundation is removed via nitric acid etching, leaving isolated gold structures within the pores.*

EXPERIMENTAL DETAILS

Figure 1 shows a schematic of the electrochemical template synthesis method for preparing single rods. One face of the porous film is coated with silver using a plasma deposition device (Anatech Hummer 10). The coated film is then placed in an electrochemical cell such that only the uncoated face is exposed to silver plating solution [14]. Additional silver metal is deposited potentiostatically until the coated face is sealed and silver rods grow part way into the film. The silver plating solution is then removed, the cell rinsed with distilled water, and then filled with Au(I) cyanide plating solution (Orotemp 24, Technic, Inc.). The deposition current is integrated to provide a continuous indication of the progress of the gold deposition. The length of the gold rods can be controlled by halting the deposition after a certain number of coulombs has passed [7]. Once the gold deposition is complete, the metal/host film composite is immersed in concentrated nitric acid to remove the silver foundation. In the majority of our studies, the host film was porous anodic aluminum oxide, which we prepare from ultrapure aluminum. Details of the aluminum anodization are given elsewhere [6,8].
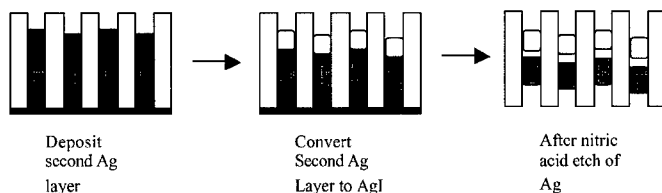
Figure 2A shows the electrochemical template synthesis scheme for metal nanoparticle pair structures. Following step C in figure 1, instead of proceeding to the Ag etch step, additional silver is deposited onto the gold layer. Gold is then deposited onto the second silver layer. The spacing between the two gold structures is determined by the thickness of the silver spacer layer. Finally, the silver foundation and spacer layers are removed via nitric acid etch.

In figure 2B, we summarize the electrochemical template synthesis of gold/silver iodide nanoparticle pair structures. Again following step C in figure 1, additional silver is deposited onto the gold layer. This second silver layer is then oxidized in the presence of an aqueous potassium iodide solution (1 M). This results in the precipitation of AgI in the vicinity of the gold layer. If the entire second layer of Ag is converted to AgI, the resulting AgI semiconductor phase is in intimate contact with the gold metal layer. However, if some of the Ag layer is left

2A: Metal Pair Synthesis

Deposit
second Ag
layer

Deposit
second Au
layer

After nitric acid
etch of Ag
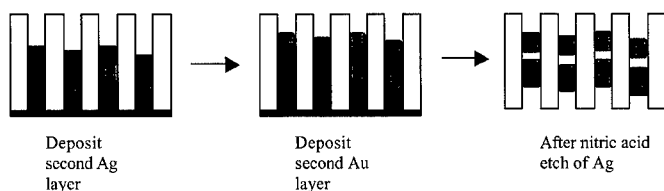
2B: Metal/Semiconductor Pair Synthesis

Deposit
second Ag
layer

Convert
Second Ag
Layer to AgI

After nitric
acid etch of
Ag

Figure 2. A. Electrochemical template synthesis of gold nanoparticle pair structures. B. Electrochemical template synthesis of gold/silver iodide nanoparticle pair structures.

unoxidized, its subsequent removal in the nitric acid etch step results in Au and AgI particles which are, on average, separated by certain distance within each pore.

In our laboratory, all electrochemical deposition and oxidation steps were performed potentiostatically using an EG&G Princeton Applied Research Model 273 potentiostat. The exposed plating area of each film was ca. 3.14 cm^2. The reference electrode in all cases was a silver chloride coated silver wire immersed in 4M KCl, and separated from the plating solution by a Vycor® porous glass junction. The counter electrode was platinum mesh (ca. 1 cm^2).

Structural characterization of the particles involved imbedding the aluminum oxide composites in resin, and microtoming sections thin enough for transmission electron microscopic (TEM) imaging. A JEOL 1200 EX TEM was used for all characterizations.

Linear optical characterization was performed using a Hitachi U3501 UV/Visible/Near-IR spectrometer, equipped with a model 210-2130 polarizer accessory. SHG measurements were performed using a mode locked titanium:sapphire laser pumped with an argon ion laser. The details of the laser setup are described elsewhere [11,15]. The basic optical setup is shown in figure 3. The thin aluminum oxide film (typically 40-50 μm in thickness) is mounted in a

source   polarizer   Sample   Filter and Monochromator (SHG expt. only)   Detector
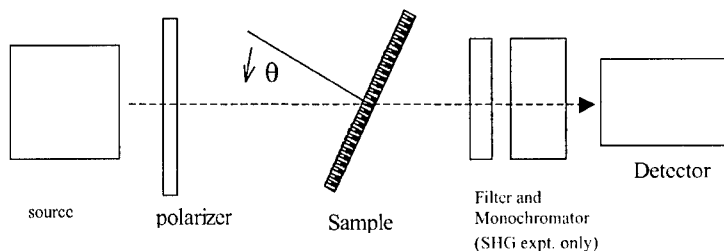
Figure 3. Schematic of the optical sample configuration for linear and nonlinear optical studies. In the figure above, the incident light is defined as p-polarized ($\phi = 0^o$) when the electric field is polarized in the plane of incidence (also plane of the page). s-polarization ($\phi = 90^o$) corresponds to the electric field polarized in the plane of the sample (perpendicular to the plane of the page).

sample holder which affords control over the incidence angle (θ, measured versus the surface normal) of the source beam. The polarizer defines the polarization angle ϕ. In the case of the SHG measurements, the incident wavelength is ca. 800 nm. A cut-off filter between the sample and detector removes the incident wavelength, and a monochromator isolates the SHG signal at ca. 400 nm [11,15].

RESULTS

Some examples of the gold nanoparticle pair structures that we have prepared via electrochemical template synthesis are shown in figure 4. These TEM images are cross sections through the template host aluminum oxide films. The template synthesis method allows for the control of metal nanoparticle dimensions and pair spacing, but only in an average sense. The standard deviation of most parameters (length, diameter, and spacing) is 10% or greater, which is certainly a lower precision than modern optical and electron beam lithographic methods can achieve. However, electrochemical template synthesis is inexpensive, and low tech enough to be executed in even modestly equipped laboratories. In spite of the shortcoming in terms of dimensional precision, the method has allowed us to perform some basic optical investigations and gain important insights into nanostructure-optical property relationships.
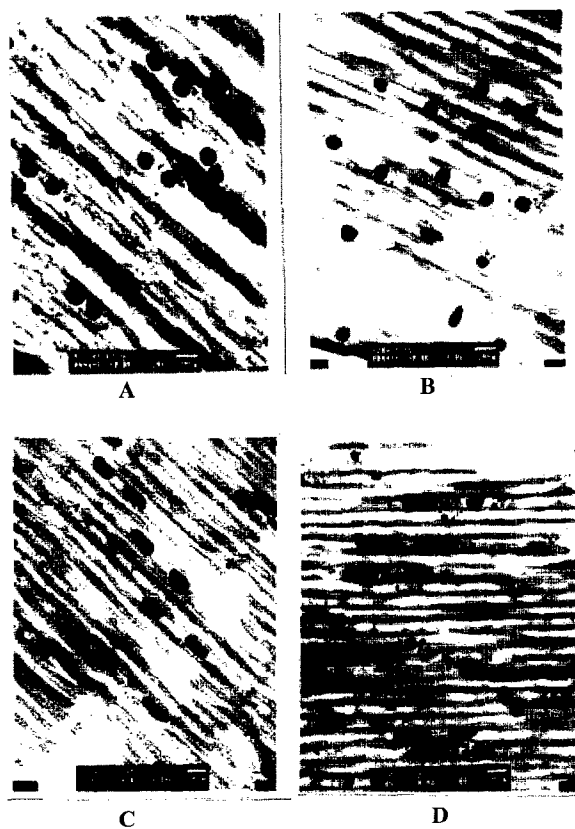
Figure 4. Gold nanoparticle pair structures prepared in porous anodic aluminum oxide via the electrochemical template synthesis method. **A.** 32 nm diameter sphere pairs, edge-edge spacing ca. 20 nm. **B.** 32 nm sphere pairs, edge-edge spacing ca. 80 nm. **C.** Centrosymmetric rod pairs (diameters = 30 ±3 nm, lengths = 70 ±10 nm, edge-edge spacing 70 ±20 nm). **D.** Non-centrosymmetric rod-sphere pairs (rod dimensions: length= 100 ±10 nm, diameter = 33 ±4 nm; sphere-like segment length = 34±5 nm, diameter = 33±4 nm). Scale bar (white bar in image caption box) 50 nm in all images.

To examine the effects of interparticle spacing on the optical spectra of metal nano-particles, we conducted polarization spectroscopy measurements on the samples corresponding to the TEM images in figures 4a and 4b. The plasmon resonance bands of the gold nanoparticle pairs were measured under p-polarization as a function of incidence angle θ. Table I summarizes the results.

**Table I. Effect of Interparticle Spacing on Plasmon Resonance Maximum**

Sample	λ_{max}(nm) $\theta = 0^{\circ}$	λ_{max}(nm) $\theta = 20^{\circ}$	λ_{max}(nm) $\theta = 30^{\circ}$	λ_{max}(nm) $\theta = 45^{\circ}$
32 nm diameter Au spheres, Separation distance 20 nm	539	543	549	558
32 nm diameter Au spheres, Separation distance 80 nm	548	548	548	548

It is clear that when the average spacing between the two spheres is small, their plasmon resonance maximum is incidence angle dependent. As θ increases, and increasing component of the incident electric field is parallel to the particle pair axis. If the induced electric field of one particle is sensed by its partner, the plasmon resonance maximum will be red-shifted. At large separations, the particles are not electromagnetically coupled, and thus their spectral maxima are independent of the incidence angle. These observations are in qualitative accord with simple quasistatic model predictions [10,15]. However, the experimental spectral bands are considerably broader than those predicted by theory.

In the case of molecular materials, second order nonlinear optical behavior is expected only when the crystalline solid (or local ensemble subject to measurement) lacks inversion symmetry [16]. One of our primary motivations for extending the template synthesis to particle pair structures was to prepare nanoscale structures that lack inversion symmetry, and then investigate their second order nonlinear optical properties. Using the optical configuration shown in figure 3, we measured the SHG signal from two sample types, centrosymmetric gold rods and non-centrosymmetric gold rod-sphere pairs. The dimensions of each system were chosen such that their linear optical properties were similar, both in terms of the position the spectral maxima, and also the absolute optical density. This was done so that local field enhancements would be similar in both systems, and thus allow us to focus specifically on nanostructure symmetry.

Figure 5 summarizes the results of the first SHG study, which involved particles of moderate aspect ratio (length/diameter), which we shall refer to as Group I. It is clear that in p-polarization, the SHG counts for the non-centrosymmetric system are significantly higher than in the case of the centrosymmetric rods. In figure 5B, the increase in SHG counts with θ are expected, as an increasing incidence angle implies a larger component of the electric field along the asymmetry axis of the pair. Neither sample showed significant SHG counts in s-polarization. In figure 6, we show an analogous set of plots for higher aspect ratio particles (which we refer to as Group II). It is interesting that in p-polarization, the SHG counts for the centrosymmetric and non-centrosymmetric systems are similar. Furthermore, both samples in Group II give significantly higher SHG counts than the samples of Group I.

While a more detailed interpretation will be given elsewhere [17], the comparison of the Group I and Group II studies suggests the following: for second order nonlinear optical behavior in nanoparticle systems, symmetry is more important when the particles are small. As the particles increase in size, second order effects such as SHG become less sensitive to symmetry. This preliminary interpretation would indicate that the well-known electric dipole approximation [16] which is the context in which the second order nonlinear optical properties of molecular systems is discussed, is not generally applicable to nanoparticle systems. This is consistent with the fact that other electromagnetic induction modes become significant as the particle dimensions
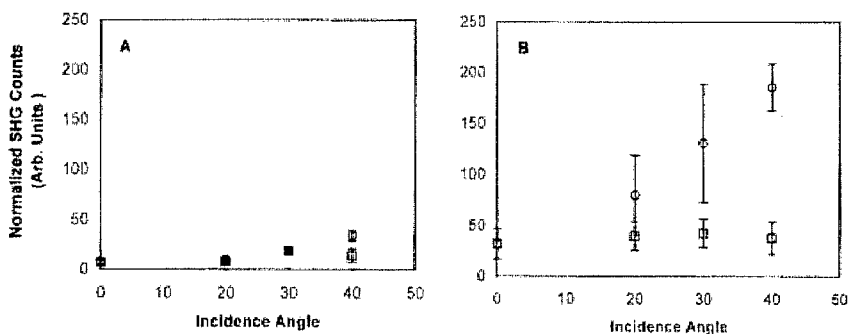
Figure 5. *SHG counts for centrosymmetric and noncentrosymmetric gold nanoparticle structures (Group I) versus incidence angle θ. Open circles correspond to p-polarization. Open squares are counts obtained in s-polarization. Error bars based on standard deviation of measurements on three different locations on film samples. All counts normalized to signal from a slurry of potassium dihydrogen phosphate crystals in decahydronaphthalene. A. Centrosymmetric rods, length = 54 ±7 nm, diameter = 30 ±4 nm. B. Non-centrosymmetric rod-sphere pairs. Rods: length = 37 ±6 nm, diameter = 26 ±3 nm. Spheroids: length = 27 ±5 nm, diameter = 26 ±3 nm. Edge-edge spacing = 22 ±8 nm.*
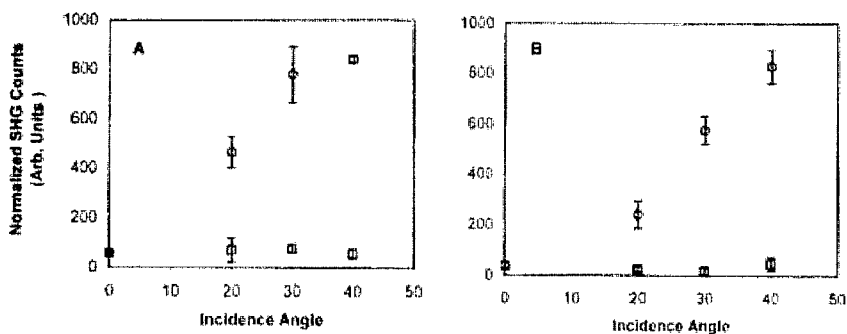
Figure 6. *SHG counts for centrosymmetric and noncentrosymmetric gold nanoparticle structures (Group II) versus incidence angle θ. Open circles correspond to p-polarization. Open squares are counts obtained in s-polarization. Error bars based on standard deviation of measurements on three different locations on film samples. All counts normalized to signal from a slurry of potassium dihydrogen phosphate crystals in decahydronaphthalene. A. . Non-centrosymmetric rod-sphere pairs. Rods: length = 100 ±10 nm, diameter = 33 ±4 nm. Spheroids: length =34 ±5 nm, diameter = 33 ±4 nm Edge-edge spacing = 57 ±13 nm. B. Centrosymmetric rods, length = 133 ±20 nm, diameter = 31 ±4 nm.*

increase. For example, the magnetic dipole and electric quadrupole oscillations can produce a second harmonic signal even from centrosymmetric particles [18]. We should note that because

the increased aspect ratio of the Group II particles caused their long axis plasmon resonance to coincide more closely with the incident laser wavelength, we considered the possibility that huge local fields may be enhancing weak magnetic dipole and electric quadrupole modes (hence, the important difference between Group I and Group II is not overall particle size, but the aspect ratio). While this remains a distinct possibility, our local field calculations, which take into account particle shape and size [19] suggest that local field enhancements are negligible.

Another approach to achieving non-centrosymmetric pair structures is for the two pair members to be composed of different materials. We originally prepared the gold/silver iodide pair structures according to the scheme in figure 2B with the intention of investigating their potential for SHG. While these systems proved too photochemically fragile for laser work, their linear optical spectra revealed other issues which are quite relevant to nanoparticle technology.

As we seek to prepare nanoparticle structures of increasing geometric and compositional complexity, two key issues are 1) the nature of the electromagnetic interaction between particles composed of different materials, and 2) in the case where the two particles are in contact, the nature of the interface between two dissimilar materials. When we first prepared gold/silver iodide particle systems, we expected the linear optical spectra to reflect a weighted sum of the two materials; the gold particle component should exhibit a plasmon resonance band near 520 nm, and the silver iodide should show a band edge and sharp exciton feature at 425 nm. However, the first spectral studies, which considered gold and silver iodide phases in intimate contact, showed gold plasmon resonance bands that were red-shifted and severely broadened. Furthermore, the silver iodide exciton peak was absent [12]. When we synthesized the particle pair such that there was a space between the metal and semiconductor phases, the gold plasmon resonance band narrowed and shifted back to its expected λ_{max} [13] (See the spectral curves in figure 7 which pertain to contacting and spaced particles).

As we were unable to model the experimental spectra assuming bulk optical properties for gold and silver iodide, and thus concluded that material cross-contamination was likely occurring. Using effective medium type theories and a modified Drude free electron model for the metal phase, we simulated both atomic level mixing and gross aggregate formation of large domains of semiconductor in the metal phase, and vice versa [13]. The simulated spectra showed red-shifting and broadening of the gold plasmon resonance similar to the experimental results.

The cross-contamination hypothesis led us to modify slightly the template synthesis scheme shown in figure 2B. After the gold layer is deposited, the gold plating solution is removed and replaced with an aqueous potassium sulfide solution. A potential sufficiently positive to cause oxidation of the gold is applied briefly, resulting in the formation of a thin layer of gold sulfide (Au_2S). Silver is then deposited onto the sulfide coated gold surface, and subsequently converted to silver iodide. The middle curve of figure 7 shows the consequences of adding a gold sulfide layer: the gold plasmon resonance band recovers its position and shape (it is nearly identical to the band corresponding to gold particles separated from the silver iodide by an air gap), but the exciton peak is still absent. Our preliminary interpretation is that the gold sulfide layer prevents contamination of the gold phase by silver or iodine atoms of the AgI phase. The persistent absence to the AgI exciton may be due to the close proximity of the metal phase (the high concentration of free electrons in the gold may promote image charges which destabilize electron-hole interactions in the semiconductor phase.
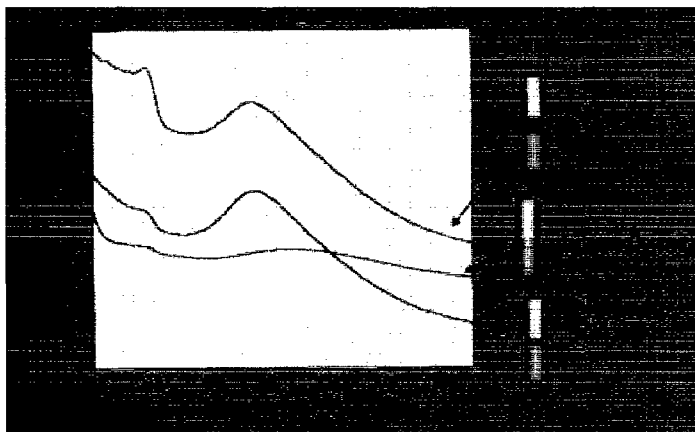
Figure 7. Linear optical spectra of gold/silver iodide nanoparticle pair structures. All spectra were obtained at normal incidence (See figure 3). Spectral curves are on same relative absorbance scale, but displaced vertically and arbitrarily for clarity.

CONCLUSIONS

The electrochemical template synthesis method offers a straightforward and inexpensive means for preparing nanoparticle pair structures. The variety of structures includes both centro- and noncentro- symmetric metal pairs, and metal-semiconductor pairs. While the method does not currently afford precise control over particle dimensions (at least compared to modern lithographic techniques), it has allowed us to gain insight into nanostructure-optical property relationships. Second order nonlinear optical properties can be achieved in nanomaterials, but the absence of inversion symmetry may be a strict requirement only when the nanoparticles are small and amenable to the dipole approximation. Complex nanostructures that involve particles composed of different materials may engender the risk of cross contamination, especially if the two phases are placed in physical contact. As we seek to prepare nanostructures with increased geometric and compositional complexity, we will need to develop synthetic strategies for controlling the interface between particles.

ACKNOWLEDGMENTS

REFERENCES

1. M.A. Hayat, *Colloidal Gold: Principles, Methods and Applications*, (Academic Press, 1989).
2. J.E. Beesley, *Proc. Royal Microscop. Soc.*, **20**, 187 (1985).
3. Faraday, M., *Philos. Trans.*, **147**, 145 (1857).
4. J.C. Hulteen and R.P. van Duyne *J. Vac. Sci. Tech.*, **13**, 1553 (1995).
5. M.J. Tierney and C.R. Martin, *J. Phys. Chem.*, **93**, 2878 (1989).
6. C.K. Preston and M. Moskovits *J. Phys. Chem.*, **92**, 2957 (1988).
7. C.A. Foss, Jr., M.J. Tierney, and C.R. Martin, *J. Phys. Chem.*, **96**, 9001 (1992).
8. C.A. Foss, Jr., G.L. Hornyak, J.A.Stockert, and C.R. Martin, *J. Phys. Chem.*, **98**, 2963 (1994).
9. N.A.R. Al-Rawashdeh, M.L. Sandrock, C.J. Seugling, and C.A. Foss, Jr., *J. Phys. Chem. B*, **102**, 361 (1998).
10. M.L. Sandrock and C.A. Foss, Jr. *J. Phys. Chem. B*, **103**, 11398 (1999).
11. M.L. Sandrock, C.D. Pibel, F.M. Geiger, and C.A. Foss, Jr., *J. Phys. Chem. B*, **103**, 2668 (1999).
12. M. El-Kouedi, M.L. Sandrock, C.J. Seugling, and C.A. Foss, Jr. *Chem. Mater.* **10**, 3287 (1998).
13. M. El-Kouedi and C.A. Foss, Jr. *J. Phys. Chem. B*, **104**, 4031 (2000).
14. N.A. Shumilova and G.V. Zutaeva, in *Encyclopedia of Electrochemistry of the Elements*, ed. A.J. Bard (Marcel Dekker, 1978).
15. M.L. Sandrock, PhD Dissertation, Georgetown University, 2000.
16. R.W. Boyd, *Nonlinear Optics*, (Academic Press, 1992).
17. M.L. Sandrock and C.A. Foss, Jr., manuscript in preparation.
18. X.M. Hua and J. I. Gersten, *Phys. Rev. B*, **33**, 3756 (1983).
19. M. Meier and A. Wokaun, *Optics Lett.*, **8**, 851 (1983).